Numerical Thermal Analysis of Six-Phase PMSMs With Single- and Double-Layer Fractional-Slot Concentrated Windings in Healthy and Faulty Cases

Wessam E. Abdel-Azim[1,2], Alejandro G. Yepes[1], Ahmed Hemeida[3,4], Ayman S. Abdel-Khalik[5], Shehab Ahmed[6], and Jesús Doval-Gandoy[1]
[1]*CINTECX*, *Universidade de Vigo*, *APET*, Vigo, Spain
[2]*Department of Electrical Engineering*, *Alexandria University*, Alexandria, Egypt
[3]*Department of Electrical Engineering and Automation*, *Aalto University*, Espoo, Finland
[4]*Department of Electrical Engineering*, *Cairo University*, Giza, Egypt
[5]*Department of Electrical and Computer Engineering*, *Sultan Qaboos University*, Muscat, Oman
[6]*CEMSE Division*, *KAUST*, Thuwal, Saudi Arabia
Email: wessam.essam@uvigo.es, agyepes@uvigo.es, ahmed.hemeida@aalto.fi, a.abdelkhalik@squ.edu.om, shehab.ahmed@kaust.edu.sa, jdoval@uvigo.es

***Abstract*—Multiphase permanent-magnet synchronous machines (PMSMs) with fractional-slot concentrated windings (FSCWs) are favored for many uninterruptible applications due to their high fault tolerance and torque density. Two different configurations are often adopted: single layer (SL) and double layer (DL). For SL, each slot is filled with one phase winding, while for DL, two phases can share the same slot. Accordingly, many research papers advise adopting SL in fault-tolerant PMSMs, rather than DL, because SL offers higher physical, thermal, and electromagnetic isolation between phases. However, the lower the thermal isolation, as for DL, the greater the heat transfer. This could be expected to reduce the temperature differences between phases, and hence the hot-spot temperatures under unbalanced conditions such as faults. Thus, the established preference of SL over DL for fault-tolerant PMSMs may be questioned, and further analysis is necessary. This paper compares the temperature distribution of six-phase PMSMs between SL and DL FSCWs under both healthy and faulty conditions, considering open-circuit and short-circuit (interturn) winding faults. For accurate results, finite-element analysis and computational fluid dynamics are employed for the loss calculation and thermal simulation, respectively.**

***Index Terms*—Fault tolerance, fractional-slot concentrated winding, six-phase permanent-magnet synchronous machine, thermal model.**

I. Introduction

Multiphase permanent-magnet (PM) synchronous machines (PMSMs) are versatilely deployed, compared with three-phase ones, in high-performance and high-reliability applications such as electric vehicles, ship propulsion, and aerospace due to their great fault tolerance, reduced torque ripple, better dc-link utilization, and multiple fault-tolerant (FT) control strategies [1]. To achieve an efficient PMSM design, the fractional-slot concentrated winding (FSCW) is adopted in the stator because it offers shorter end-winding length, higher fill factor and higher torque density compared with distributed winding [2]. Generally, FSCW can be designed with two different arrangements: single layer (SL) or double layer (DL). In principle, each slot is occupied with one coil side for SL, while two coil sides can be included in each slot for DL [2], [3]. SL produces higher harmonic content in back-electromotive force (back-EMF) and magnetomotive force (MMF) than DL, and thereby has a potentially higher overload torque capability than DL [3]. In addition, the greater electric, magnetic, and thermal isolation between SL phases is usually considered to make SL a more suitable candidate for FT PMSMs than DL [2]–[6]. On the other hand, DL exhibits lower PM eddy-current and core losses and torque ripple [3].

For safety-critical applications, the fault tolerance should be ensured in multiphase PMSMs. Among various fault kinds, open-phase faults (OPFs) and short-circuit faults (SCFs) are commonly investigated in FT PMSMs [1]. Some fault types in multiphase drives, e.g., open-/short-circuit switch faults and high-resistance connections, can be adapted as OPFs [1]. Some freedom degrees are missed under OPFs depending on the fault locations, and thereby torque ripple usually increases if the machine control is not adapted. With FT control, an enhanced performance can be achieved, in terms of maximizing torque production with ripple-free torque and minimizing stator copper losses, by optimizing the phase currents [7]. However, some phases having higher rms current values than others tend to overheat, and hence, the torque capability is constrained with the thermal limits [8]. Operating PMSMs beyond their thermal limits can lead to insulation degradation and an increased risk of PM demagnetization [1]. Thermal analysis under OPFs is therefore crucial for identifying localized hot-spot regions, enabling the development of effective FT control strategies that ensure better temperature distribution and reasonable machine derating [4], [8]–[10].

This work was supported in part by the Government of Galicia under the grant GPC-ED431B 2023/12, and in part by the Spanish State Research Agency MCIN/AEI/10.13039/501100011033/FEDER-UE under projects CNS2022-135773 and PID2022-136908OB-I00.

The thermal behavior of FT PMSMs under SCFs should also receive a great attention, because of the large resulting currents and losses. Most severely, one or more turns of a specific phase may be short-circuited, which is termed as an inter-turn fault (ITF). The fault current in an ITF is inversely proportional to the number of shorted turns [11] and depends on its location, with closer to the slot opening being more critical [1], [12]. For each phase driven by a separate full-bridge (FB) inverter (commonly adopted in PMSMs [5], [6], [11]), applying a terminal short circuit (SC) through the two upper/lower switches is the simplest remedial action to tolerate ITFs [12]. The circulating SC current produces a flux linkage opposing the PM flux linkage in the shorted turns [11]. Alternatively, the mutual interaction between the faulty and healthy phases can be exploited to alleviate the SC current in the shorted turns. To do so, the healthy-phase currents should be adapted such that the mutual flux linkage of the healthy phases nulls the PM flux linkage in the shorted turns [7]. This method is more feasible for DL than for SL since the mutual coupling between phases is higher [3]. Accordingly, the remarks in [2]–[7] about the SL isolation being preferred for FT PMSMs are questionable.

To assess the thermal performance of a machine design, there are two main approaches, as follows. The well-known lumped-parameter thermal networks are computationally efficient and offers reasonable accuracy only when thermal parameter estimation and loss calculations are accurate [13]. On the other hand, numerical methods based on either finite-element analysis (FEA) or computational fluid dynamics (CFD) give more precise thermal prediction, just at the cost of increased computational burden [4], [8].

Many research works have used numerical analysis to assess the thermal performance of FT PMSMs either with SL [4] or DL [8] under healthy and faulty conditions. Bianchi *et al.* [5] perform 2D thermal FEA of a five-phase PMSM with SL under OPFs while keeping the rated copper losses. To achieve higher postfault torque, not only the healthy-phase currents surpass the rated value, but also the hot-spot temperature is higher than that of rated healthy condition. On the contrary, Jiang *et al.* [8] evaluate the thermal performance of a five-phase PMSM with DL under minimum-loss (ML) current-control strategy while respecting the maximum temperature rise of rated healthy operation. In this manner, the healthy-phase currents, under various OPF cases, can exceed the rated machine current to increase the torque, while maintaining the hot-spot temperature of rated normal operation. Furthermore, an FT control method with an even temperature distribution between faulty and healthy modules of a modular PMSM is proposed in [10]. To achieve this, an electromagnetic-thermal coupled model is used in the iterative algorithm to generate the optimum module current. In the same context, the ML and maximum-torque (MT) current-control strategies are compared at rated healthy conditions from the thermal point of view in [4], [9]. It has been found that MT exhibits higher maximum temperature rise than ML, because higher copper losses are obtained under MT to achieve the rated healthy torque. All these works have investigated the temperature fields of multi-phase PMSMs with a certain winding design under various FT control methods without studying the influence of the winding configuration (SL or DL) on the thermal distribution. Namely, the thermal coupling between DL phases may play a crucial role in improving the heat exchange between phases sharing the same slot. This could affect the temperature distribution and the hot-spot temperatures substantially, which requires further research.

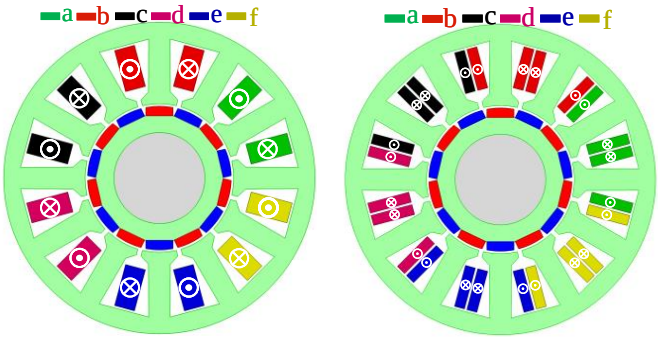

(a) (b)

Fig. 1. Cross-sectional view for winding layouts of the FSCW 6PMSMs. (a) SL. (b) DL.

In this paper, the thermal behavior of both SL and DL windings is compared for six-phase PMSMs (6PMSMs) under different scenarios such as healthy, OPF, and ITF. The CFD analysis is performed using Ansys Fluent for each studied case. Furthermore, Ansys Maxwell is used to obtain the loss model, which provides the heat sources in the thermal model.

II. FSCW 6PMSM Design

For high-speed applications, a relatively low pole number is typically selected among the possible FSCW slot-pole combinations [14]. Since close values of slot and pole numbers achieve a high fundamental winding factor and a high torque density [14], the 12-slot/10-pole and 12-slot/14-pole combinations are usually considered in the FSCW PMSM design. Nevertheless, the 12-slot/14-pole PMSM offers better field-weakening capability, higher power density, and greater values of maximum speed, compared with the 12-slot/10-pole counterpart [15]. Moreover, it also results in reduced torque ripple and lower material cost [14]. Accordingly, the 12-slot/14-pole FSCW 6PMSM is considered as a case study. It is designed with a high self-inductance such that the SC current for a phase SC at rated speed is limited to the rated machine current. This design approach is favored for FT PMSMs without interrupted operation under SCFs [6]. The optimization methodology outlined in [15] is employed to determine the machine design parameters provided in Table I. For SL [see Fig. 1(a)], each slot has one coil side with $160\ \mathrm{turns/coil}$. As for DL [see Fig. 1(b)], each slot is filled with two coil sides either of the same phase or of two different phases with $80\ \mathrm{turns/coil}$, and thereby the cross-slot mutual coupling is higher than that in SL layout [3], [6]. For a fair

TABLE I
DESIGN DETAILS OF THE FSCW PMSM

Parameter	Value	Parameter	Value
Stator outer diameter (mm)	130	Stator slot number	12
Stator inner diameter (mm)	62	Rotor pole number	14
Airgap length (mm)	1	Turns/slot number	160
PM width (mm)	10.68	Rated power (kW)	2
Stack length (mm)	60	Rated torque (Nm)	9.75
Core steel material	M235-35	Rated speed (r/min)	2000
PM material	N42sh	Rated phase voltage (V)	110

comparison, both layouts are wound with a symmetrical six-phase arrangement. As illustrated in [16], asymmetrical configurations are not feasible for SL machines with a 12-slot/14-pole topology. It is noteworthy that symmetrical configuration achieves higher postfault torque than other arrangements [17]. Besides symmetrical winding layout, each phase winding is fed by an FB inverter so as to separately control each phase [5], [6], [11].

III. ELECTROMAGNETIC FEA

In this section, the electromagnetic model for both machines is developed in Ansys Maxwell to acquire the losses, which will then be required for thermal analysis. Fig. 2 shows the no-load back-EMF of both windings with trapezoidal waveforms. The optimum phase currents can be generated using the generalized strategy in [7]. This strategy is employed here because it not only minimizes the stator copper loss with ripple-free torque, but also considers many possibilities such as nonsinusoidal back-EMF, any number of phases, different winding connections, various operating modes, and any fault locations. While retaining most of the previous features, the current-reference generation method in [18] can also be adopted if the additional functionalities are desired such as extending the torque range with minimal torque ripple, including current and torque-ripple limitations, and enabling automatic transition from overload to steady-state operation.

The heat sources in PMSMs are mainly stator copper loss P_{cu}, core loss P_{core}, and PM loss P_{PM}. The loss calculations adopted in Ansys Maxwell are well-established and detailed in [4], [8]. All the loss model parameters are listed in Table II.

A. Healthy Case

For a fair comparison, the same operating conditions (rated torque and speed) are applied for both machines. With the closed-form solution in [7], the phase currents, depicted in Fig. 3, are obtained for both designs considering the two different back-EMFs in Fig. 2. It should be emphasized that no constraint of zero phase-current summation is applied to the solution of [7], since each phase is driven by an FB inverter. It can be seen from Fig. 3 that the phase-current rms value for SL is 3.68% lower than for DL at the same torque due to the higher harmonic content in the back-EMF for SL. Ansys Maxwell is used to obtain the losses of each layout by exciting the electromagnetic model with the corresponding phase currents. Table III shows the calculated loss components

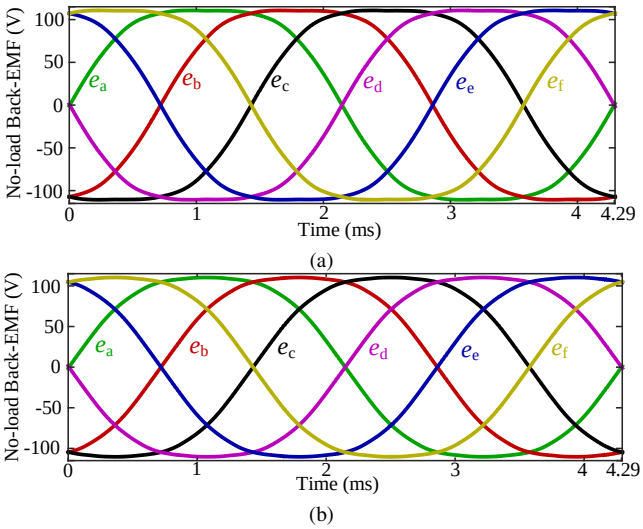

Fig. 2. No-load per-phase back-EMF of the FSCW 6PMSMs at rated speed. (a) SL. (b) DL.

TABLE II
LOSS MODEL PARAMETERS

Parameter	Symbol	Value
Copper conductivity (S/m)	σ_{cu}	$58 \cdot 10^6$
PM conductivity (S/m)	σ_{PM}	$0.6 \cdot 10^6$
Hysteresis loss coefficient	K_{h}	172.042
Eddy-current loss coefficient	K_{c}	1.368
Excess loss coefficient	K_{e}	1.765

of each winding layout. DL exhibits 9.50% lower total losses compared with SL. This is mainly attributed to the lower harmonic components in the DL MMF. It is noteworthy that the PM eddy-current losses of both layouts are much lower than the other losses.

B. OPF Case

In this case, both machines are simulated under the same torque and speed (i.e., rated) as in the healthy case, keeping the machine operation without derating, while phase a is open-circuited ($i_{\mathrm{a}} = 0$). Similarly, the procedures of the healthy case are replicated here to obtain the optimal healthy-phase currents shown in Fig. 4. It is worth highlighting that DL still results in 9.24% lower total losses than SL, as indicated in Table III.

C. ITF Case

To ensure a fair comparison of the resulting losses in both machines under the ITF case, the same number of shorted turns (specifically, 10 turns of phase a) is adopted in both machines. The fault resistance between shorted turns is assumed to be $20\,\mathrm{m}\Omega$. As recommended in [11], [12], to alleviate the SC current, an external SC is applied across the faulty-phase terminals by turning on the upper/lower switches of the corresponding FB inverter. The healthy-phase currents are the same as in the healthy case shown in Fig. 3, but discarding i_{a}. It is clear from Table III that DL produces higher total losses than SL by 19.85% due to the higher resulting fault current

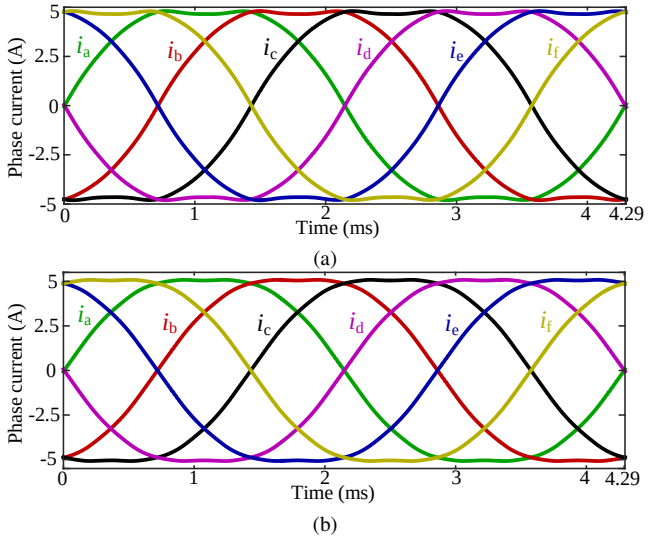

Fig. 3. Phase-current references of the FSCW 6PMSMs under the healthy case at rated torque and speed. (a) SL. (b) DL.

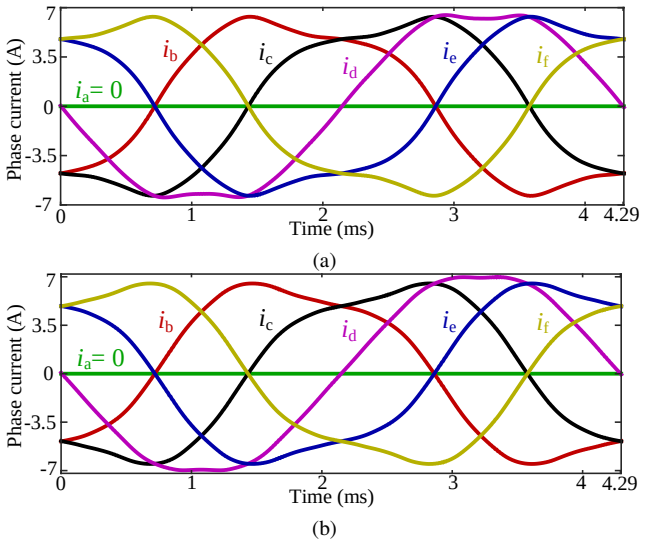

Fig. 4. Phase-current references of the FSCW 6PMSMs under an OPF in phase a at rated torque and speed. (a) SL. (b) DL.

TABLE III
COMPARISON OF LOSS COMPONENTS FOR BOTH LAYOUTS AT RATED TORQUE AND SPEED UNDER THREE DIFFERENT SCENARIOS

Scenario	P_{cu} (W)		P_{core} (W)		P_{PM} (W)		Total losses (W)	
	SL	DL	SL	DL	SL	DL	SL	DL
Healthy	47.67	47.01	64.86	55.80	7.00	5.36	119.53	108.17
OPF	58.77	57.91	69.70	61.10	8.92	5.69	137.39	124.70
ITF	68.09	99.67	53.10	46.67	6.55	6.76	127.74	153.10

in DL compared with SL. This may be due to the mutual flux linkage of DL healthy phases reinforcing the PM flux linkage in shorted turns, and further research into the actual causes may be conducted in the future.

IV. CFD-BASED THERMAL ANALYSIS

The loss model provided in Ansys Maxwell is coupled to the thermal model via Ansys Workbench. The CFD-based thermal analysis is carried out using Ansys Fluent. The thermal properties of the used materials are given in Table IV. Regarding the air-gap modeling, a turbulent flow occurs, when the air-gap Reynolds number Re_{g} is greater than the critical Reynolds number Re_{crit} (as usual in rotating electric machines). Otherwise, a laminar flow is considered in the air gap with the air thermal conductivity [19]. For the turbulent flow, the air gap is modeled as a solid with an equivalent air-gap thermal conductivity λ_{g}, which can be calculated by [4], [19], [20]

$$\begin{aligned} \lambda_{\mathrm{g}} &= 0.069\eta^{-2.9084} Re_{\mathrm{g}}^{0.4614\ln(3.33361\eta)}; \\ Re_{\mathrm{g}} &= \tfrac{\omega_{\mathrm{r}} R_{\mathrm{ro}} \delta}{\nu} > Re_{\mathrm{crit}} = 41.2\sqrt{\tfrac{R_{\mathrm{si}}}{\delta}}; \eta = \tfrac{R_{\mathrm{ro}}}{R_{\mathrm{si}}} \end{aligned} \tag{1}$$

where ω_{r} is the angular rotor velocity, R_{ro} is the rotor outer radius, R_{si} is the stator inner radius, η is th radius ratio, δ is the air-gap length, and ν is the air kinematic viscosity. The heat exchange on the stator outer surface is a combination of natural and forced convection, with the latter resulting from the air blown by a fan. Accordingly, the mixed convection coefficient of the stator surface can be expressed as [4], [8]

$$h_{\mathrm{st}} = 9.73 + 14 v_{\mathrm{st}}^{0.62} \tag{2}$$

where v_{st} is the air velocity on the stator surface ($v_{\mathrm{st}} = 8\,\mathrm{m/s}$), which can be estimated from the rotor operating speed [21]. The calculated convection coefficient of the stator surface is $h_{\mathrm{st}} = 60.55\,\mathrm{W/m^2/K}$. Since the hot-spot temperature typically locates at the end windings [4], [10], [19], heat transfer at end-space surfaces should be taken into account. The convective heat transfer coefficient of the end-space surface can be computed by [20]

$$h_{\mathrm{end}} = 15.5 + 4.495 v_{\mathrm{end}} \tag{3}$$

where v_{end} is the air velocity at the end space, which equals $\omega_{\mathrm{r}} R_{\mathrm{ro}}$. From (3), $h_{\mathrm{end}} = 43.74\,\mathrm{W/m^2/K}$.

A. Healthy Case

The generated losses of both machines at the same rated torque and speed from the electromagnetic model are injected as heat sources in the thermal model to obtain the steady-state temperature distribution. Fig. 5 shows the temperature distribution of both designs. The maximum temperatures are located at the end windings. Both layouts exhibit uniform temperature distributions across phases due to the equal phase-current rms values under healthy conditions displayed in Fig. 3. However, due to the thermal coupling between DL phases, the DL hot-spot temperature reduces by 9.02% with respect to SL, as shown in Fig. 5. To clarify whether the decrease in hot-spot temperature for DL is due to its lower losses or to its different thermal conductance across its heat transfer paths, another simulation is performed. Namely, the input losses of SL are manually forced to be the same as for DL in Ansys Fluent, as indicated in Table V. From Table V and Fig. 6, DL still keeps a lower hot-spot temperature than SL

TABLE IV
THERMAL MODEL PARAMETERS

Material	Thermal conductivity (W/m/K)	Mass density (Kg/m^3)	Heat capacity (J/Kg/K)
Copper	387.6	8978	381
Insulation	0.3	2000	502
M235-35	22	7600	460
N42sh	6.45	7600	460.55
Air gap	1.94	1.1	1006

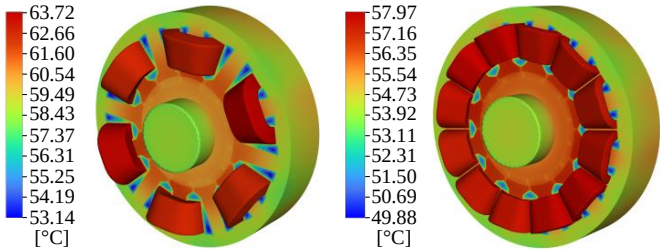

Fig. 5. Temperature distribution under the healthy case at rated torque and speed. (a) SL. (b) DL.

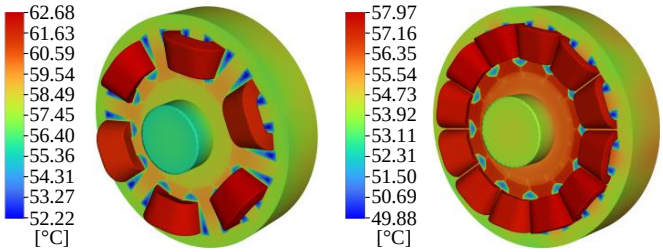

Fig. 6. Temperature distribution under the healthy case for the same input losses and rated speed. (a) SL. (b) DL.

(by 7.51%). This reveals that the lower maximum temperature for DL is mainly due to the heat exchange between the phases sharing the same slot, and not to its reduction in losses.

B. OPF Case

Opening phase a makes it a passive phase, while the other healthy phases are active ones. The heat transfer between active and passive phases can be better exploited for DL than for SL due to the physical sharing of two DL phases within the same slot. As depicted in Fig. 7, DL outperforms SL by lowering the maximum temperature by 11.04%. Moreover, if the losses of DL are manually forced as equal inputs for both SL and DL, as shown in Table V and Fig. 8, the maximum temperature for DL is still lower (by 9.30%). This confirms the relation of the DL temperature decrease with the (higher) thermal conductances of DL between phases, regardless of the losses. It can also be noted from Fig. 7 that the hot-spot temperature of both designs is located at phase d, which has the highest phase-current rms value (see Fig. 4).

C. ITF Case

Fig. 9 displays the temperature fields of both machines under the ITF condition discussed in Section III-C. The hot-

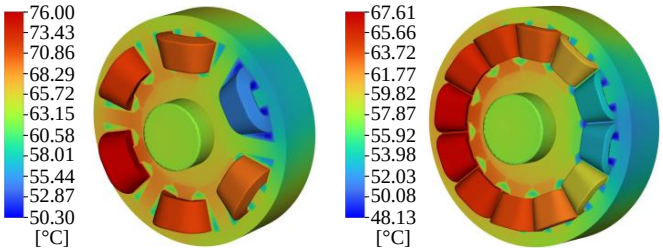

Fig. 7. Temperature distribution under the OPF case with phase a open at rated torque and speed. (a) SL. (b) DL.

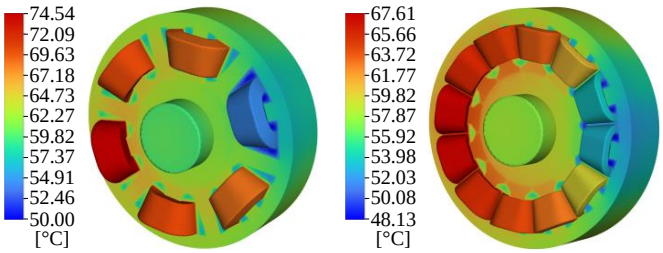

Fig. 8. Temperature distribution under the OPF case (with phase a open) for the same input losses and rated speed. (a) SL. (b) DL.

spot temperature is higher than for the healthy and OPF cases. Consequently, reducing this temperature is essential to avoid problems like PM demagnetization, insulation degradation, and thermal runaway [1]. In contrast to the maximum temperature of OPF case, the faulty phase in ITF case produces the highest temperature with respect to other healthy phases due to the excessive SC current in the faulty phase. It can be observed from Fig. 9 that the hot-spot temperature is higher for DL than for SL, mainly due to the higher copper losses of DL compared with SL in this case (see Table III). Nevertheless, if the losses of SL are manually defined to match the DL losses, DL showcases a 10.19% lower hot-spot temperature than SL, as depicted in Fig. 10 and Table V. This is thanks to the greater thermal coupling between healthy and faulty phases for DL.

V. CONCLUSIONS

In this study, the steady-state temperature distribution of FSCW 6PMSMs with both SL and DL windings is investigated using CFD-based thermal model under the prospective operating cases (healthy, OPF, and ITF). Under each case, both layouts are thermally compared twice: one at the same rated torque and speed, and the other at the same input losses. Thanks to the reduction of the MMF harmonics for DL, it achieves reduced total losses by 9.50% and 9.24% under healthy and OPF conditions, respectively, compared with SL. However, under the ITF case, it generates 19.85% higher losses than SL, possibly due to the mutual flux linkage of healthy phases boosting the PM flux in shorted turns. Thermally, the hot-spot temperature is notably reduced by 9.02% and 11.04% (at the same rated torque and speed) under healthy and OPF cases, respectively, compared with SL. Under the ITF case, a much higher hot-spot temperature